JACS
JOURNAL OF THE AMERICAN CHEMICAL SOCIETY

ARTICLE

pubs.acs.org/JACS

Controlled Synthesis of Tuned Bandgap Nanodimensional Alloys of PbS_xSe_{1-x}

Javeed Akhtar,[†,∥] Mohammad Afzaal,[‡] Mateusz Banski,[§] Artur Podhorodecki,[§] Marcin Syperek,[§] Jan Misiewicz,[§] Ursel Bangert,[⊥] Samantha J. O. Hardman,[¶] Darren M. Graham,[¶] Wendy R. Flavell,[¶] David J. Binks,[¶] Sandra Gardonio,[#,Δ] and Paul O'Brien*[,†]

[†]School of Chemistry and Materials Science Centre, The University of Manchester, Oxford Road, Manchester M13 9PL, United Kingdom

[‡]Center of Research Excellence in Renewable Energy, King Fahd University of Petroleum and Minerals, Dhahran, 31261 Saudi Arabia

[§]Institute of Physics, Wroclaw University of Technology, Wybrzeze Wyspianskiego 27, 50-370 Wroclaw, Poland

[⊥]Materials Science Centre, The University of Manchester, Grosvenor Street, Manchester M1 7HS, United Kingdom

[¶]School of Physics and Astronomy and the Photon Science Institute, The University of Manchester, Oxford Road, Manchester M13 9PL, United Kingdom

[#]SuperESCA beamline, Sincrotrone Trieste S.C.p.A., S.S. 14 Km 163.5, 34012 Basovizza, Trieste, Italy

Supporting Information

ABSTRACT: Truly alloyed PbS_xSe_{1-x} ($x = 0-1$) nanocrystals (~5 nm in size) have been prepared, and their resulting optical properties are red-shifted systematically as the sulfur content of the materials increases. Their optical properties are discussed using a modified Vegard's approach and the bowing parameter for these nanoalloys is reported for the first time. The alloyed structure of the nanocrystals is supported by the energy-filtered transmission electron microscope images of the samples, which show a homogeneous distribution of sulfur and selenium within the nanocrystals. X-ray photoelectron spectroscopy studies on ligand-exchanged nanocrystals confirmed the expected stoichiometry and various oxidized species.

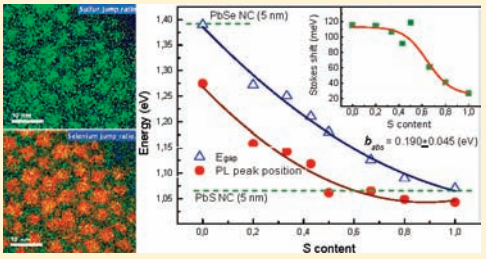

INTRODUCTION

Lead chalcogenides, PbE (E = S, Se, Te), as nanocrystals (NCs) have been of considerable interest of late.[1] One driving force is the recently discovered phenomenon of multiple exciton generation (MEG),[2] which could ultimately lead to more efficient solar energy conversion.[3,4] Recent efforts to synthesize binary lead chalcogenide nanostructures with well-defined geometrical shapes (e.g., as tubes,[5] rods,[6] or wires[7]) have opened up new possibilities for developing strategies for light harvesting. Sargent and co-workers have reported solution-processed infrared responsive photovoltaic devices based on PbS quantum dots and confirmed oxidation at the surface of the nanoparticles (NPs).[8] Oxidation products such as $PbSO_4$ and $PbSO_3$ were shown to affect the open circuit voltage of the devices. Lead chalcogenide NCs also show great promise in the field of thermoelectric devices,[9] telecommunications,[10] and as biological markers.[11]

Ternary lead sulfide selenide (PbS_xSe_{1-x})[12] NCs have not been extensively studied in contrast to the parent binary materials PbS and PbSe.[13] Alloyed semiconductor nanomaterials provide an alternative approach for bandgap control in additional to the size-dependent quantum confinement effects; and they give access to families of material with distinct properties. The properties of alloys vary with composition making it possible to tune the bandgap while maintaining a similar small size as in CdS_xSe_{1-x} NCs.[13] The size of NCs can be of significant importance when making functional devices. Also, PbS_xSe_{1-x} NCs can yield more efficient PV devices through a combination of J_{SC} and V_{OC} unavailable in either of the parent PbS or PbSe.[14] The stoichiometric ratio of S/Se in NCs of such ternary materials has, on occasion,[14] been found to be greater than the injected precursor ratio due to differing intrinsic reactivities of the chalcogenide sources used for example TMS (bis(trimethylsilyl)sulfide) and TOPSe (trioctylphosphine selenide).[14] The TMS, used as the sulfur source, is far more reactive and is rapidly consumed; probably in the nucleation phase. It is hence important to devise a synthetic scheme to produce the desired alloy (homogeneous) structures. For homogeneous alloys, the growth rates of the two constituent materials must be close to equal and the growth conditions for one constituent cannot impede the uniform growth of the other.[13] This approach has been successfully used in the tailored synthesis of complex oxides such as lead zirconium titanate by choosing precursors for different metals with similar decomposition temperatures.[15]

Received: October 20, 2010
Revised: February 1, 2011
Published: March 21, 2011

dx.doi.org/10.1021/ja200750s | J. Am. Chem. Soc. 2011, 133, 5602–5609

Table 1. PL and Transition Energy of First Excitonic Peaks and Composition of Alloy NCs

sample code	composition (x)[a] in PbS_xSe_{1-x}	PL peak position (nm)	transition energy $1S_e - 1S_h$ (nm)
S-1	0	971	892
S-2	0.20	1083	975
S-3	0.33	1090	992
S-4	0.43	1105	1024
S-5	0.50	1175	1050
S-6	0.67	1169	1100
S-7	0.80	1188	1137
S-8	1	1200	1159

[a] Where $x = (S/(S + Se))$.

Detailed information about the internal structures of ternary NCs is often not available, but some reports do give valuable information.[16] In the present work, we have attempted to overcome the differences in reactivity of S and Se sources by using reagents with similar structures, and by inference reactivity, (TMS and TMSe). Tunable emission, dependent on composition, has been systematically demonstrated over the composition range of the PbS_xSe_{1-x} ($x = 0-1$) NCs. As would be expected, the emission wavelength red-shifts gradually with increased S content. Detailed transmission electron microscopy (TEM) studies confirmed the growth of homogeneous alloyed PbS_xSe_{1-x} structures. It is important to form a distinction between a gradient alloy and homogeneous NCs, as gradient alloy NCs have different optical properties than those of homogeneous ones. An insight into the surface properties of alloyed structures by X-ray photoelectron spectroscopy (XPS) further confirms the composition. Finally, we have explored the effect of alloy composition on the optical properties of homogeneous NCs.

EXPERIMENTAL SECTION

All of the chemicals were bought from Sigma Aldrich Ltd. and used as received. Bis(trimethylsilyl)selenide was acquired from Fluorochem Ltd. The olive oil used in this study was purchased from Tesco supermarket, UK Ltd. and its composition is given in Supporting Information. The solvents were distilled prior to use.

Synthesis of PbS_xSe_{1-x} Nanoalloys. PbS_xSe_{1-x} were prepared similar to the method reported for PbS.[17] Typically, 0.92 g (4 mmol) of PbO was dissolved in 12.5 mL of olive oil along with 1 mL of oleic acid and 1 mL of octadecene in a three neck flask fitted with a thermometer. The contents of the flask were heated to 100 °C and kept at this temperature for 1 h. Then the flask was filled with N_2 gas and the temperature was raised to 130 °C. When the temperature was stabilized, controlled amounts of TMS and TMSe (Table 1) dissolved in 0.5 mL of octadecene and 1 mL of olive oil was rapidly injected into the lead solution. Growth time for each experiment was kept constant for 90 s after which the reaction was quenched with cold water. The NCs were precipitated by adding 20 mL of anhydrous acetone and centrifuged for 10 min. The obtained brown-black residue was resuspended in 5 mL of toluene and again 20 mL of acetone was added and centrifuged for 5 min.

Characterization. X-ray powder diffraction patterns were obtained using a Bruker D8 AXE diffractometer (Cu Kα). TEM samples were prepared by evaporating a dilute toluene solution of the nanoparticles on carbon-coated copper grids (S166-3, Agar Scientific) and a Philips Technai Transmission Electron microscope was used to obtain TEM images of the nanoparticles. X-ray photoemission spectroscopy was performed on the nanoalloys on the SuperESCA beamline, Sincrotrone, Trieste, Italy.

For optical measurements, PbS_xSe_{1-x} samples were dissolved in toluene and placed in a quartz cuvette. The absorbance spectra were measured using a halogen lamp and HORIBA Jobin Yvon iHR320 monochromator combined with an InGaAs detector working in lock-in technique. An air-cooled argon laser was used as a source of excitation beam (514 nm wavelength, 1 mW average power) in the photoluminescence (PL) experiments. The emission was collected in a 90° configuration and dispersed on HORIBA Jobin Yvon Triax 550 monochromator and recorded by HORIBA Jobin Yvon liquid nitrogen-cooled InGaAs linear CCD camera. Simultaneously, the transmission of the exciting beam through the sample was recorded to calculate the relative quantum yield according to the equation $RQY_X = ((QY_X)/(QY_0)) = ((abs_0)/(abs_X))((IntPL_X)/(IntPL_O)) \cdot 100\%$, where abs_x is the absorbance of sample at 514 nm wavelength and $IntPL_X$ is a integrated PL intensity of sample PbS_xSe_{1-x} under excitation at 514 nm. For time-resolved PL experiments, a Ti:Sapphire oscillator (Coherent Mira-HP-Duo) pumped by a Nd:YVO4 DPSS CW laser was used as a source of the excitation beam of 740 nm, 100 kHz, and ~1 mW average power. The PL decay signal was recorded by Hamamatsu Streak Cameras coupled to an Acton SP2360 spectrograph.

RESULTS AND DISCUSSION

Compositionally tuned PbS_xSe_{1-x} NCs were prepared by adding specific amounts of the sulfur and selenium (TMS or TMSe) to a PbO solution at 130 °C (for details see Table 1). The minimal lattice mismatch of 2% makes PbS and PbSe logical candidates for forming a substitutional alloy (Figure S1 of the Supporting Information). Powder XRD of the NCs suggested ternary-alloyed materials at all compositions of the halite structure and all of the characteristic reflections for the alloys fall between the values for PbS and PbSe. TEM studies indicate the formation of monodispersed NCs, for example 5.5 ± 0.8 nm (sample S-1) and 5.4 ± 0.6 nm (sample S-6) in size (Figure S2 of the Supporting Information). To establish that the PbS_xSe_{1-x} samples are alloyed, energy-filtered TEM (EFTEM) analysis was carried out using a Tecnai F30 equipped with a Gatan imaging filter. Structural investigations by TEM studies on samples S-5 and S-7 showed that the resulting NPs are truly alloyed with almost equal distribution of sulfur and selenium.

Part a of Figure 1 shows a TEM image of the alloyed NCs (sample S-5) and the corresponding parts b and c of Figure 1 show *ZLP* images of different resolution acquired to perform electron energy loss analysis. Energy dispersive X-ray analysis (EDAX) spectra of single particles (sample S-5), as shown in part d of Figure 1, show the presence of selenium and sulfur, however, due to the small size of the probe around 10 Å, the S- and Se-distributions within individual crystals could not be obtained. Moreover, both the sulfur and the selenium EDX signals occur in the 2−3 KeV region, and it is difficult to make a distinction between them (part d of Figure 1). Energy-filtered imaging was employed to eliminate effects due to variations in the thickness of the TEM specimens. Rather than acquiring elemental maps, jump ratio maps were recorded, in which the post-edge intensity of the respective edge was divided by the pre-edge intensity. The energy window for Se was chosen as 10 eV, centered around the Se−M−edge at 57 eV for the post-edge image, and from 30 to 40 eV for the pre-edge image. For S, the energy window width was 30 eV, starting just after the S−L−edge at 165 eV for the post-edge image and from 120 to 160 eV for the pre-edge image (parts a−c of Figure 2). The acquisition time for the energy-filtered images was between 15 and 25 s. Examples of jump ratio maps for Se and S, as well as of the zero-loss distribution in

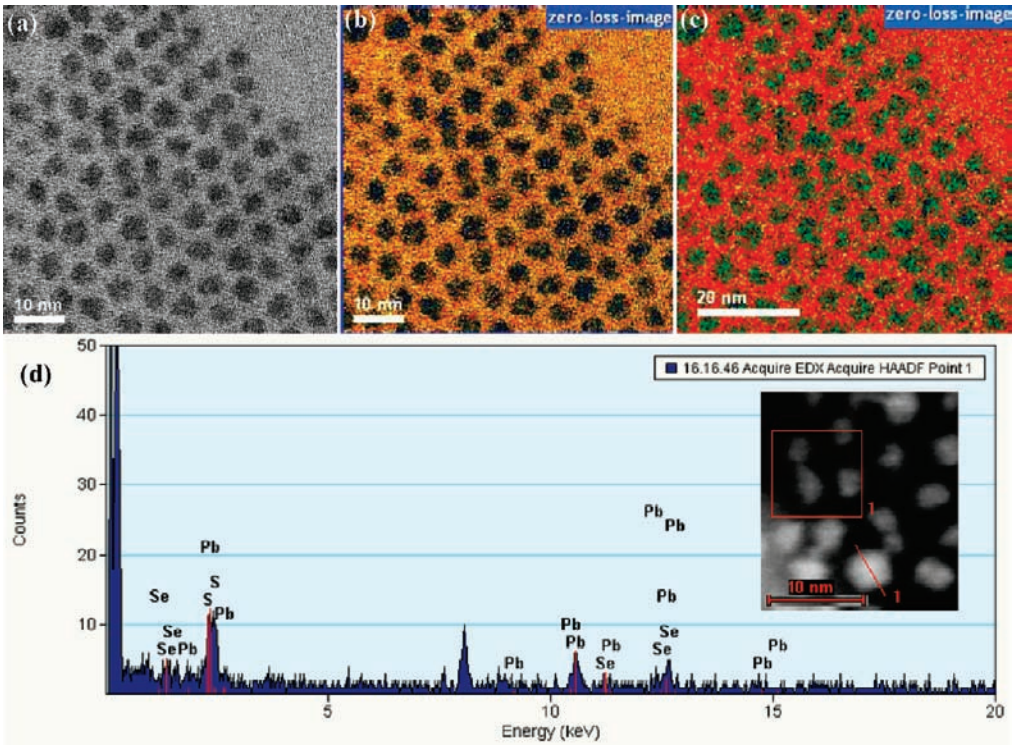

Figure 1. (a) TEM image of PbS_xSe_{1-x} nanocrystals for sample S-5; (b) and (c) zero loss images of selenium and sulfur, respectively; and (d) EDX profile graph with an insert of a dark field image of alloyed NCs.

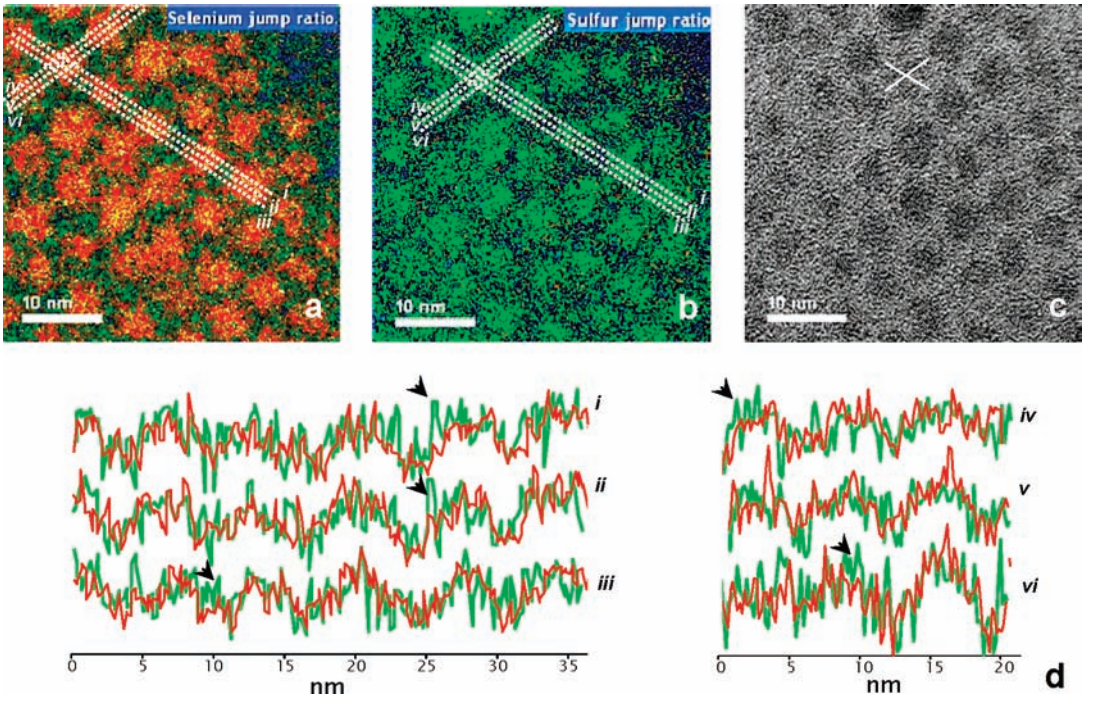

Figure 2. (a) Se and b) S jump ratio map (for details see text), (c) zero loss image. White lines (i−iii) and (iv−vi) in (a) and (b) denote positions of two groups of line scans along two particle rows in oriented in different directions. The white cross in (c) and the position of crossing lines in (a) and (b) denote the same particle, d) intensity profiles of the Se (red) and S (green) jump ratio along scan lines (i−vi); the arrows point to positions, where the shapes of the Se and S profiles deviate from each other.

approximately the same areas are shown in parts a−c of Figure 2. Because of a slight specimen drift between image acquisitions, the particles in the three images are not in identical positions. The following analysis has been adjusted for this; the location of the crossed lines in each image denotes the center of the same particle. The NCs assume positions on a near-hexagonal 'lattice'.

dx.doi.org/10.1021/ja200750s |J. Am. Chem. Soc. 2011, 133, 5602–5609

Table 2. Peak Assignments and Details for Samples S-5 and S-6[a]

	core level		
	Pb 4f	Se 3p	S 2p
	Sample S-5		
proportional composition	19	0.49	1
species;	PbS and PbSe;	PbSe;	PbS;
label and position (eV);	Pb1 138.6 and 143.5;	Se1 162.3 and 168.1;	S1 161.2 and 162.4;
percentage of core level	51%	100%	27%
	oxidized PbS;		oxidized PbS;
	Pb2 139.6 and 144.4;		S3 167.0 and 168.2;
	Pb3 142.0 and 147.9;		S4 168.7 and 169.9;
	49%		52%
			neutral S;
			S2 163.6 and 164.8;
			21%
	Sample S-6		
proportional composition	3.3	0.86	1
species;	PbS and PbSe;	PbSe;	PbS;
label and position (eV);	Pb1 138.0 and 142.9;	Se1 162.1 and 167.9;	S1 161.2 and 162.4;
percentage of core level	45%	100%	29%
	oxidized PbS;		oxidized PbS;
	Pb2 139.0 and 143.9;		S3 166.9 and 168.1;
	38%		S4 168.6 and 169.8;
			S5 169.4 and 170.6;
	neutral Pb;		S6 172.9 and 174.1;
	Pb4 137.0 and 141.9;		71%
	17%		

[a] Peak labels correspond to those in Figures S3 and S4 in the Supporting Information.

The false-color EFTEM images 2a and b give a first impression of homogeneous elemental distribution, however, closer analysis is required. Detailed analysis was carried out to ascertain the composition of the various NCs. The dashed white lines with numbers (i−iii) and (iv−vi) in parts a and b of Figure 2 are the positions where intensity profiles were taken. Three parallel, closely spaced line scans were taken along a row of particles; for rows in two different directions (60° to each other); scan directions are from left to right. Closely spaced intensity profiles along the centers of particles and at a ∼1 nm distance on either side of centers were attained to reveal information about the homogeneity of the group VI element within individual particles. Line scans (i−iii) are displayed in the left-hand and (iv−vi) in the right-hand panel of part d of Figure 2. The red and green lines refer to Se and S, respectively. In spite of the noise in the signal, it is clear that the Se and S distributions follow the same trend, that is the distributions assume similar shapes for each particle; as would be expected for a homogeneous alloy. The actual shape of each particle (faceting) does not appear to be of importance to the homogeneity. In the case of core−shell segregation, a 'top-hat' distribution would be expected for the shell-element and a center-peak distribution for the core-element. The top hat distribution would become broader and the center-peak distribution narrower as the scan line proceeds along the peripheries of the particles, that is, in scans i, iii, iv, and iv (Figure 2). Arrows in the line scans point to positions, where Se and S intensities might be seen as deviating from each other, although the noise level of the scans prohibits a clear decision on this. If the NPs had a well developed core−shell structure, deviations would be expected in all three profiles in the same positions; which is not the case. Hence we conclude that in a number of the NCs some segregation may occur, with S tending to accumulate off center, but that there is no development of a clear core−shell structure. More than 50% of the particles appear homogeneously alloyed.

Two samples S-5 and S-6 were investigated by XPS (details in Figures S3 and S4 of the Supporting Information). It has previously been discovered that the presence of the long insulating oleic acid alkyl chain causes samples to charge in XPS experiments.[17] Therefore, resulting NPs were ligand exchanged with ^{n}butylamine and deposited on an ITO-coated glass substrate. High-resolution spectra of the Pb 4f, S 2p, and Se 3p core levels are shown in Figures S3 and S4 of the Supporting Information, and peak assignments and positions are listed in Table 2. A Shirley-type background was subtracted and Gaussian/Lorentzian sum functions were used to fit the line shapes. The spin−orbit splitting of the doublets was set as 4.9 eV for the Pb 4f peaks, 1.2 eV for the S 2p peaks, and 5.8 eV for the Se 3p peaks. The intensity ratio was set as 4:3 for the Pb 4f doublets and 2:1 for the

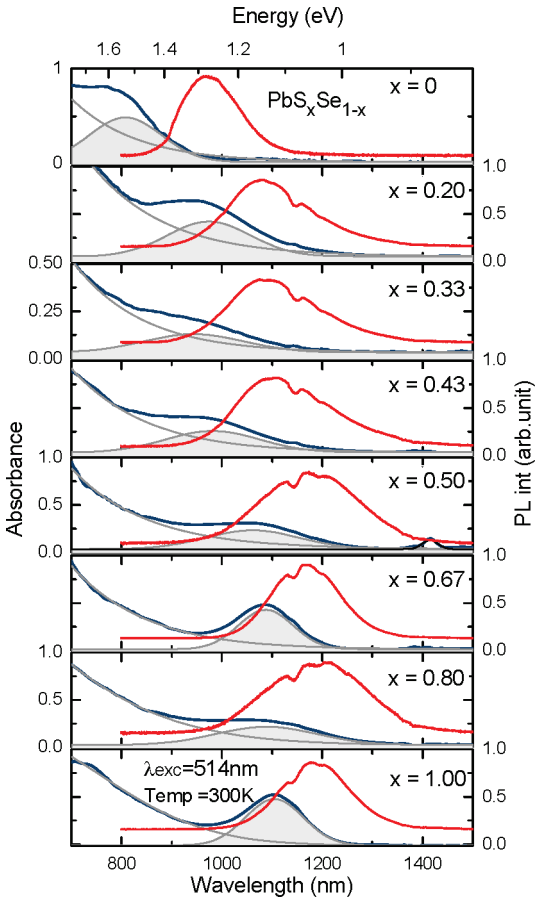

Figure 3. Absorbance (blue) of PbS_xSe_{1-x} measured at 300 K for x in the range 0−1. The first excitonic absorption transition is fitted by a Gaussian function and shaded for clarity. PL spectra (red) measured at room temperature, excited wavelength λ_{exc} = 514 nm.

S 2p and Se 3p doublets. The photon energy used was 250 eV, so the kinetic energy of electrons detected corresponds to a sampling depth of ~1.7 nm.[18] Using the areas of the S 2p and Se 3p core level spectra and the photoionisation cross sections,[19] it was found that the samples had an Se/S ratio of 0.49:1 (sample S-5), and 0.86:1 (sample S-6).

Both samples appeared to have only one state of Se present, with a binding energy consistent with assignment to PbSe, but multiple states of S including neutral, and strongly oxidized species. In both samples S as found in PbS made up ~28% of the S present, and S as found in oxidized PbS made up around 50%. The remaining S component varied between samples. The sample S-5 contained some neutral sulfur, whereas in the sample S-6 only PbS and oxidized sulfur components were found. The Pb 4f spectra also show a similar large proportion of oxidized species. It is impossible to distinguish between the Pb as found in PbS and as found in PbSe because the peak positions are so similar,[20] but in both samples approximately half the Pb is present as either PbS or PbSe. The oxidized species present in the samples are due to exposure of the surfaces of the NCs to the air after synthesis, an effect which has been previously observed in PbS NCs.[17] The binding energy of the edge of the valence band is equivalent to the gap between the Fermi level and the valence band of a substance. This value was measured as 1.0 ± 0.2 eV for the S-5 sample and 0.8 ± 0.2 eV for the S-6 sample. In both samples, the Fermi level is closer to the conduction band than the valence band, so both samples are *n*-type semiconductors.

To better understand the internal structure of the alloy, we have investigated the influence of the composition of PbS_xSe_{1-x} NCs on their optical properties. Absorption and photoluminescence have been measured for all of the samples (Figure 3). The absorption spectra are characterized by a well-resolved band related to the first excitonic transition within the NCs overlapped with a long tail of scattered light.[21] Increased sulfur content of the NCs caused a significant red shift of these absorption bands. The absorption band positions for PbSe and PbS samples were 1.39 and 1.07 eV respectively, which agree with literature data[22] for NCs of ~5 nm. These findings suggest that the size of NCs is kept constant throughout the synthesis. Moreover, estimated in this way the NCs radii are in agreement with our structural data, thus the composition related to the S/Se ratio is the main factor influencing the changes in the optical properties of our NCs.

Similar changes are seen in the PL spectra, and the emission bands also move to longer wavelengths with an increase in sulfur content (Figure 3). The full width at half-maximum (fwhm) calculated for PbSe and PbS NCs are 143 and 174 meV, respectively. These values are comparable to the results from other reports.[23] For alloyed samples, spectral broadening is higher and the fwhm reaches a maximal value of 235 meV for x = ~0.5. This broadening could be strictly ascribed to the distortion in crystal structures associated with alloy formation. However, the fwhm increase is about 25−45%, thus a homogeneous distribution of the additional component in ternary alloy, rather than phase separation into binary PbS and PbSe clusters, is expected in the internal structure of our NCs.

To discuss the influence of nanoalloy composition on the emission intensity, the relative PL quantum yields (RQY_X) were calculated for the samples (Figure S5 of the Supporting Information). A monotonic increase in RQY_X was observed with increasing the sulfur content. There was only exception for the $PbS_{0.8}Se_{0.2}$ sample, in which $RQY_{0.8}$ drops by 80%. We speculate that this effect is related to formation of additional defect states, which strongly reduce the PL intensity and consequently decrease $RQY_{0.8}$ in our $PbS_{0.8}Se_{0.2}$ sample.

Figure 4 shows both the PL peak positions and energy gaps obtained from absorbance measurements as a function of NC composition. The values of E_g have been determined from the absorption spectra by calculating their second derivatives and taking the position of its first minimum. In Figure 4 it can be seen that E_g and the PL peak position of the alloyed samples varies continuously and smoothly in the range between E_g of PbSe and PbS NCs. This is a further evidence for a true alloying for PbS_xSe_{1-x} in the NCs.

The differences between absorption and emission spectra (Stokes shifts, Δ_{SS}) have been compared for all samples to gain a better insight into their physical properties. Different contributions to the Stokes shift in NCs have been discussed in the literature: size distribution effects (exciton migration),[24] electron−hole interactions (excitonic fine structure),[25] the Franck−Condon shift[26] (in weak and strong electron−phonon coupling regimes), or finally the existence of surface traps with energies in the middle of the optical gap of idealized NCs. We excluded exciton migration effects by investigation of samples at low concentration. It has been also shown that the Franck−Condon shift in this kind of material is equal to

dx.doi.org/10.1021/ja200750s |*J. Am. Chem. Soc.* 2011, 133, 5602–5609

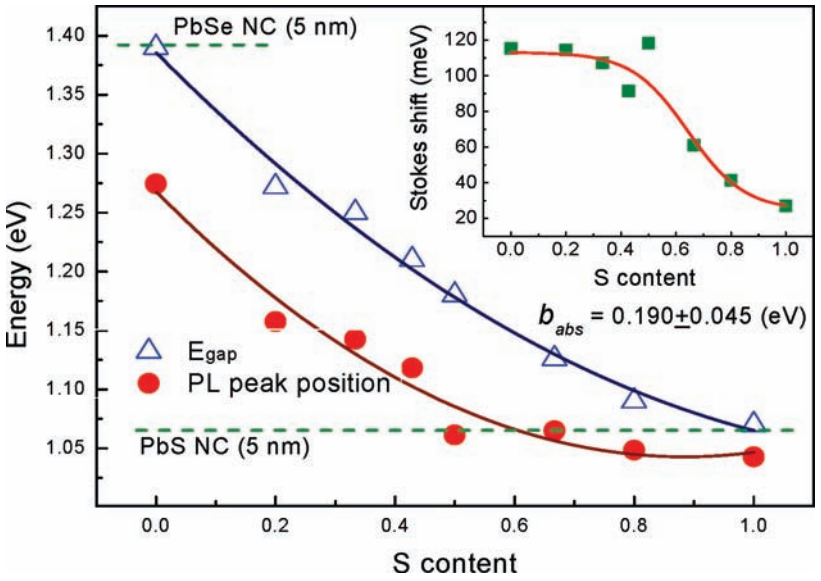

Figure 4. Relation of energy gap (empty triangles) and PL peak position (filled circle) determined from absorbance and PL spectra to the PbS_xSe_{1-x} QD composition. The insert shows a calculated Stokes shift.

~15 meV, which is much smaller than in our case.[26] Moreover, it has been shown that the contribution to the Stokes shift from the electron−hole interaction is even lower, on the order of a few meV.[25] Thus, all of these contributions can be excluded from our considerations. However, it has already been shown that the near-edge energy spectrum of 3 nm PbSe NCs is composed of many energy levels characterized by different oscillation strenghts.[27] Thus, the contribution of particular energy levels to absorption and emission spectra can be different giving rise to the observed Stokes shift. It is proposed that this mechanism is responsible for Δ_{SS} = 115 meV observed for our PbSe samples, which is in good agreement with the Stokes shift measured by Lifshitz et al. (Δ_{SS} = 100 meV for 4 nm PbSe NCs).[24]

The influence of the PbS_xSe_{1-x} composition on the nonresonant Stokes shift is presented in the insert of Figure 4 and the obtained values of 115 and 27 meV at the extreme are characteristic of pure PbSe or PbS NCs, respectively. Sigmoidal Boltzmann functions have been used to well-fit the S-shaped variation of Δ_{SS} values of the alloyed NCs.

The compositional effects on the optical properties of NCs are presented in a modified Vegard's model. This law was initially proposed to describe the linear relation of the properties of many alloy materials, especially variations in lattice constants, but also the changes of the energy gap of a semiconductor alloy as a function of their composition. However, in some classes of semiconductor materials it is only a first approximation and a modified equation (Eq.1) taking into account a nonlinear effect, called optical bowing, is necessary:

$$E_{gC}(x) = xE_{gA} + (1-x)E_{gB} - bx(1-x) \qquad \text{(Eq.1)}$$

In Eq.1, E_{gA} and E_{gB} are the intrinsic energy gap of initial binary semiconductors and E_{gC} is the energy gap of the alloy material ($C = xA + (1-x)B$). The nonlinear property variation is described by parameter b (b_{abs} for absorption edge, b_{PL} for PL peak) and its value depends on electronic and structural parameters: various electronegativities and atomic radii of the ions, and also the different lattice constants of the A and B binary structures.[28] The S and Se atoms possess similar atomic radii (1.00 and 1.19 Å) and electronegativities (2.58 and 2.55); hence the crystal mismatch of PbS and PbSe is small (~2%) and the nonlinearity is not expected to be particularly significant in this case. It should be mentioned that optical bowing could be additionally influenced by quantum confinement and changes of QD size. On the basis of the fit of Eq.1 to E_g of NCs of various compositions presented in Figure 4 the value of the bowing parameter, (to the best of our knowledge, determined for the first time) is b_{abs} = 0.190 ± 0.045 eV for PbS_xSe_{1-x} alloy NCs. As expected, it is much smaller than 0.29 eV for CdS_xSe_{1-x}[13] and 2 eV for $B_xGa_{1-x}As$,[29] and the relationship between E_g and x becomes almost linear. The bowing parameter from the PL peak position was also calculated and equals b_{PL} = 0.287 ± 0.064 eV. This b_{PL} gives the possibility to design NCs with desired size and tunable emission wavelength by changing NCs composition.

To investigate the influence of PbS_xSe_{1-x} stoichiometry on excited carrier kinetics photoluminescence lifetime measurements have been performed and the results are shown in Figure 5. The obtained PL decays have been fitted by a stretched exponential function defined as

$$I_{PL}(t) = I_0\frac{\beta}{\tau}\left(\frac{t}{\tau}\right)^{\beta-1}\exp\left(-\left(\frac{t}{\tau}\right)^{\beta}\right) \qquad \text{(Eq.2)}$$

where τ is the PL lifetime, β is the disorder parameter, and I_0 is a constant. The investigated systems are characterized by τ and β, which is close to 1 for exponential relaxation pathway (e.g. in well-defined structure) and approaches 0 for complex relaxation (e.g. in disordered materials). The parameters obtained for our NCs are summarized in the insert of Figure 5. The good homogeneity of our NCs is reflected in the β parameter, which is above or close to 0.90 (marked by the dashed blue line) for all but one of the samples. The exception is sample S-5, which has a β value more than two standard deviations less than the average. We note that the PL peak position and Stokes shift also lie significantly off trend for this sample (Figure 4) and that the XPS

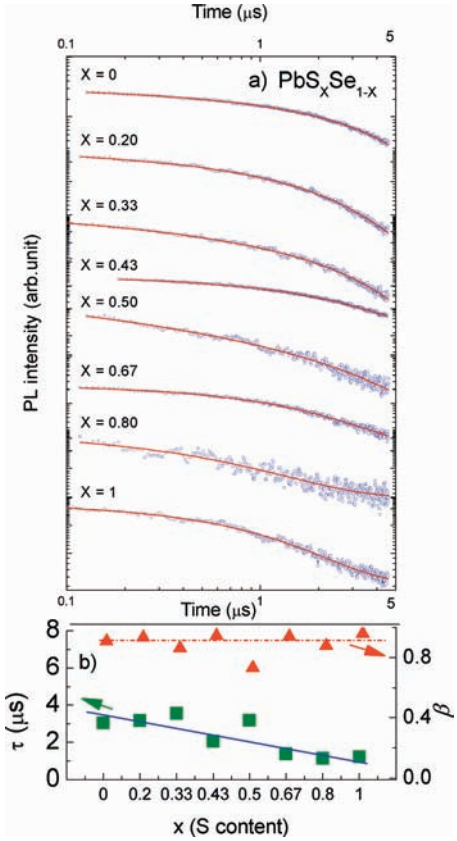

Figure 5. a) PL decay transients for the PbS_xSe_{1-x} nanoalloys; b) the PL lifetime, τ (squares) and disorder parameter, β (triangles) as a function of S content. The dashed line corresponds to the average disorder parameter and the full line to a fit of Vegard's law to the lifetimes.

measurements described above also found a significant deviation from stoichiometry for this sample, all of which suggests that S-5 is anomalous. However, for all of the samples τ decreases from $\sim$3 μs down to $\sim$1 μs as x increases from 0 to 1, and this follows Vegard's law as shown in Figure 5. This monotonous change in τ with x and the absence of a second time constant indicative of the presence of two separate phases supports the conclusion that the investigated samples, with the possible exception of S-5, are homogeneously alloyed PbS_xSe_{1-x} NCs.

CONCLUSIONS

In summary, a facile route is reported for the preparation of monodispersed alloyed NCs of PbS_xSe_{1-x}. Through the use of TMS and TMSe, the composition of the ternary NCs can be easily controlled. Homogenous distribution of sulfur and selenium within alloyed NCs is shown by EFTEM studies. Optical investigation further supports the formation of alloyed NCs rather than core/shell structures. In addition, the variations of absorption and emission energies are well fitted with Vegard's equation and for the first time the bowing parameter is determined to be equal to $b_{abs} = 0.190 \pm 0.045$ eV. The same equation was used to fit also the PL lifetimes. Hence, for alloyed NCs we are able to control energy gaps and PL dynamics by changing the NCs composition while keeping the size of NCs constant.

ASSOCIATED CONTENT

Supporting Information. Composition of olive oil, X-ray powder diffraction, transmission electron microscopy images, and X-ray photoelectron spectra of samples. This material is available free of charge via the Internet at http://pubs.acs.org.

AUTHOR INFORMATION

Corresponding Author
paul.obrien@manchester.ac.uk

Present Addresses
[‖]Nanoscience and Materials Synthesis Laboratory, Department of Chemistry, Quaid-i-Azam University, Islamabad, Pakistan.
[Δ]University of Nova Gorica Vipavska 11c, 5270 Ajdovscina, Slovenia.

ACKNOWLEDGMENT

Authors would like to thank the EPSRC, UK, for funding and Michal Baranowski for help with PL decay experiments. A. P. would like to acknowledge Iuventus Plus program (no. IP2010032570) for financial support. J.A. thanks higher education commission of Pakistan (HEC) for a Ph.D. studentship. We thank Silvano Lizzit for his assistance in performing the XPS measurements at the SuperESCA beamline, Sincrotrone Trieste. The research leading to these results has received funding from the European Community's Seventh Framework Programme (FP7/2007-2013) under grant agreement no. 226716.

REFERENCES

(1) (a) Trindade, T.; O'Brien, P.; Zhang, X.; Motevalli, M. *J. Mater. Chem.* **1997**, *7*, 1011. (b) Trindade, T.; O'Brien, P.; Zhang, X. *Chem. Mater.* **1997**, *9*, 523. (c) Afzaal, M.; Ellwood, K.; Pickett, N. L.; O'Brien, P.; Raftery, J.; Waters, J. *J. Mater. Chem.* **2004**, *14*, 1310. (d) Afzaal, M.; O'Brien, P. *J. Mater. Chem.* **2006**, *16*, 1113. (e) Berhanu, D.; Govender, K.; Smyth-Boyle, D.; Archbold, M. L.; Halliday, D.; O'Brien, P. *Chem. Commun.* **2006**, 4709. (f) Henry, C. L.; O'Mahony, F.; Akhtar, J.; Afzaal, M.; O'Brien, P.; Haque., S. A. *J. Am. Chem. Soc.* **2010**, *132*, 2743.

(2) (a) Ellingson, R. J.; Beard, M. C.; Johnson, J. C.; Yu, P.; Micic, O. L.; Nozik, A. J.; Shabaev, A.; Efros, A. L. *Nano Lett.* **2005**, *5*, 865. (b) Nozik, A. J. *Chem. Phys. Lett.* **2008**, *457*, 3.

(3) Luther, J. M.; Law, M.; Beard, M. C.; Song, Q.; Reese, M. O.; Ellingson, R. J.; Nozik, A. J. *Nano Lett.* **2008**, *8*, 3488.

(4) Beard, M. C.; Ellingson, R. J. *Laser Photonics Rev.* **2008**, *2*, 377.

(5) Tong, H.; Zhu, Y. J.; Yang, L.-X.; Li, L.; Zhang, L. *Angew. Chem., Int. Ed.* **2006**, *45*, 7739.

(6) (a) Acharya, S.; Gautam, U. K.; Sasaki, T.; Bando, Y.; Golan, Y.; Ariga, K. *J. Am. Chem. Soc.* **2008**, *130*, 4594. (b) Ziqubu, N.; Ramasamy, K.; Rajasekhar, P. V. S. R.; Revaprasadu, N.; O'Brien, P. *Chem. Mater.* **2010**, *12*, 3817.

(7) Talapin, D. V.; Yu, H.; Shevchenko, E. V.; Lobo, A.; Murray, C. B. *J. Phys. Chem. C* **2007**, *111*, 14049.

(8) Klem, E. J. D.; MacNeil, D. D.; Levina, L.; Sargent, E. H. *Adv. Mater.* **2008**, *20*, 3433.

(9) Martin, J.; Nolas, G. S.; Zhang, W.; Chen, L. *Appl. Phys. Lett.* **2007**, *90*, 222112.

(10) Rogach, A. L.; Eychmüller, A.; Hickey, S. G.; Kershaw, S. V. *Small* **2007**, *3*, 536.

(11) Wang, S.; Zhang, X.; Mao, X.; Zeng, Q.; Xu, H.; Lin, Y.; Chen, W.; Liu, G. *Nanotechnology* **2008**, *19*, 435501.

(12) (a) Brumer, M.; Kigel, A.; Amirav, L.; Sashchiuk, A.; Solomesch, O.; Tessler, N.; Lifshitz, E. *Adv. Funct. Mater.* **2005**, *15*, 1111. (b) Kigel, A.; Brumer, M.; Sashchiuk, A.; Amirav, L.; Lifshitz, E. *Mater. Sci. Eng., C* **2005**, *25*, 604.

(13) (a) Swafford, L. A.; Weigand, L. A.; Bowers, M. J., II; McBride, J. R.; Rapaport, J. L.; Watt, T. L.; Dixit, S. K.; Feldman, L. C.; Rosenthal, L. C. *J. Am. Chem. Soc.* **2006**, *128*, 12299. (b) Bailey, R. E.; Nie, S. M. *J. Am. Chem. Soc.* **2003**, *125*, 7100. (c) Zhong, X. H.; Feng, Y. Y.; Knoll, W.; Han, M. Y. *J. Am. Chem. Soc.* **2003**, *125*, 13559. (d) Lovingood, D. D.; Ovler, R. E.; Strouse, G. F. *J. Am. Chem. Soc.* **2008**, *130*, 17004. (e) Pan, A. L.; Yang, H.; Yu, R. C.; Zou, B. S. *Nanotechnology* **2006**, *17*, 1083.

(14) Ma, W.; Luther, J. M.; Zheng, H.; Wu, Y.; Alivisatos, P. *Nano lett.* **2009**, *9*, 1699.

(15) (a) Jones, A. C.; Leedham, T. J.; Wright, P. J.; Williams, D. J.; Crosbie, M. J.; Davies, H. O.; Fleeting, K. A.; O'Brien, P. *J. Eur. Ceram. Soc.* **1999**, *19*, 1431. (b) Fleeting, K. A.; O'Brien, P.; Otway, D. J.; White, A. J. P.; Williams, D. J.; Jones, A. C. *Inorg. Chem.* **1999**, *38*, 1432. (c) Jones, A. C.; Leedham, T. J.; Davies, H. O.; Fleeting, K. A.; O'Brien, P.; Crosbie, M. J.; Wright, P. J.; Williams, D. J.; Lane, P. A. *Polyhedron* **2000**, *19*, 351.

(16) (a) Beaulac, R.; Archer, P. I.; Ochsenbein, S. T.; Gamelin, D. R. *Adv. Funct. Mater.* **2008**, *18*, 3873. (b) Beaulac, R.; Schneider, L.; Archer, P. I.; Bacher, G.; Gamelin, D. R. *Science* **2009**, *325*, 973. (c) Santra, P. K.; Viswanatha, R.; Daniels, S. M.; Pickett, N. L.; Smith, J. M.; O'Brien, P.; Sarma, D. D. *J. Am. Chem. Soc.* **2009**, *131*, 470.

(17) Akhtar, J.; Malik, M. A.; Thomas, J.; O'Brien, P.; Wijayantha, K. G. U.; Dharmadasa, R.; Hardman, S. J. O.; Graham, D. M.; Spencer, B. F.; Stubbs, S. K.; Flavell, W. R.; Binks, D.; Sirotti, F.; El Kazzid, M.; Silly, M. *J. Mater. Chem.* **2010**, *20*, 2336.

(18) Tanuma, S.; Powell, C. J.; Penn, D. R. *Surf. Interface Anal.* **1991**, *17*, 927–939.

(19) Yeh, J.-J.; Lindau, I. *At. Data Nucl. Data Tables* **1985**, *32*, 1–155.

(20) Shalvoy, R. B.; Fisher, G. B.; Stiles, P. J. *Phys. Rev. B* **1977**, *15*, 1680.

(21) Kang, I.; Wise, F. W. *J. Opt. Soc. Am. B* **1997**, *14*, 1632.

(22) (a) Zhang, J.; Jiang, X. *Appl. Phys. Lett.* **2008**, *92*, 141108. (b) Gokarna, A.; Jun, K.-W.; Khanna, P. K.; Baeg, J.-O.; Seok, S. I. *Bull. Korean Chem. Soc.* **2005**, *26*, 1803.

(23) (a) Liu, T. Y.; Li, M.; Ouyang, J.; Zaman, M. Z.; Wang, R.; Wu, X.; Yeh, C.-S.; Lin, Q.; Yang, B.; Yu, K. *J. Phys. Chem. C* **2009**, *113*, 2301. (b) Kigel, A.; Brumer, M.; Maikov, G. I.; Sashchiuk, A.; Lifshitz, E. *Small* **2009**, *5*, 1675.

(24) Lifshitz, E.; Brumer, M.; Kigel, M.; Sashchiuk, A.; Bashouti, M.; Sirota, M.; Galun, E.; Burshtein, Z.; LeQuang, A.; Ledoux-Rak, I.; Zyss, J. *J. Phys. Chem B* **2006**, *110*, 25356.

(25) An., J. M.; Franceschetti, A. *Nano Lett.* **2007**, *7*, 2129.

(26) Franceschetti, A. *Phys. Rev. B* **2008**, *78*, 075418.

(27) Leitsmann, R.; Bechstedt, F. *ACS Nano.* **2009**, *11*, 3505.

(28) Wu, J.; Walukiewicz, W.; Yu, K. M.; Ager, J. W.; Haller, E. E.; Lu, H.; Schaff, W. *J. Appl. Phys. Lett.* **2002**, *80*, 4741.

(29) Jenichen, A.; Engler, C. *Phys. Status Solidi B* **2007**, *244*, 1957.